UCRL 2423

UNCLASSIFIED

UNIVERSITY OF CALIFORNIA

Radiation Laboratory

BERKELEY, CALIFORNIA

DISCLAIMER

UCRL-2423
Unclassified-Physics Distribution

UNIVERSITY OF CALIFORNIA

Radiation Laboratory

Contract No. W-7405-eng-48

ON THE LOW-ENERGY PION-NUCLEON INTERACTION

O. Heinz
(Thesis)

November, 1953

Berkeley, California

ON THE LOW-ENERGY PION-NUCLEON INTERACTION

Table of Contents

ON THE LOW-ENERGY PION-NUCLEON INTERACTION

O. Heinz
(Thesis)

Radiation Laboratory, Department of Physics
University of California, Berkeley, California

November, 1953

ABSTRACT

The production cross section for positive pions produced at 0^{o} to the 339-Mev proton beam in the reaction $p + p \rightarrow \pi^{+} + p + n$ was measured at several energies in the neighborhood of 21.5 Mev pion energy. A pion leaving the target with this energy has the same velocity as a nucleon also leaving the target at 0^{o}. A strong pion-nucleon interaction at low relative energies could then produce an appreciable effect on the shape of the pion spectrum. Measurements of the relative and of the absolute production cross section were made. No appreciable rise was observed in the relative cross section in this region and the absolute value was found to be in agreement with the values obtained by earlier experimenters.

ON THE LOW-ENERGY PION-NUCLEON INTERACTION

O. Heinz
(Thesis)

Radiation Laboratory, Department of Physics
University of California, Berkeley, California

November, 1953

I INTRODUCTION

Brueckner and Watson[1,2] pointed out that some information about the low-energy pion-nucleon interaction might be obtained from a measurement of the pion-production cross section in the reaction $p + p \rightarrow \pi^+ + p + n$. If one considers the pions leaving the target at 0^o to the incident proton beam, there is a pion energy for which the velocity of the pion may be equal to the velocity of one of the product nucleons. We thus have a situtation in which the pion and one of the nucleons, say the neutron, are traveling in the same direction with very low relative energy. This is closely analogous to the reaction $p + p \rightarrow \pi^+ + d$, in which the proton and neutron have low relative energy and thus interact to form the deuteron. This case has been studied in considerable detail by Brueckner and Watson[1] theoretically, and by Cartwright, Richman, Whitehead and Wilcox[3] experimentally. At the appropriate pion energy for deuteron formation, they find a susbtantial increase in the pion-production cross section which they attribute to the strong attractive interaction of the final nucleons.

This paper describes an attempt to investigate the pion-nucleon coupling by a measurement of the pion-production cross section in the energy region of low relative pion-nucleon velocity. An attractive interaction would tend to increase the cross section, whereas a repulsive interaction would tend to have the opposite effect.

II GENERAL DESCRIPTION OF EXPERIMENT

The pions of interest have an energy of about 21.5 Mev (See Section V, B). A measurement of the relative production cross section of positive pions in this energy region was undertaken using a CH_2-carbon subtraction method.

A thin CH_2 target (0.28 g/cm^2) and a somewhat thicker C target (0.99 g/cm^2) were exposed successively in the external proton beam of the 184-inch cyclotron. Positive pions leaving the target at approximately 0° to the proton beam are bent through 180° in a magnetic field and then stopped in the detector as shown in Fig. 1.

The brass channel serves as shielding against background particles. It also limits to $\pm 4^\circ$ the angular spread of pions that reach the target. The detector consists of a 200 μ Ilford C-2 Nuclear Emulsion embedded in an aluminum absorber as shown in Fig. 2.

The positive pions coming to rest in the emulsion can be easily identified by their characteristic decay into a μ^+ at the end of their range. By sampling the population of stopped pions at various depths of absorber we can determine, as a function of energy, the number of pions/cm^2 Mev entering the front face of the absorber. Further details about this detection scheme are given in the next section. The cross section per unit energy interval per unit solid angle $\frac{d\sigma}{dT\,d\Omega}$ is then given by this expression (See Sec. III, H),

$$\frac{d\sigma}{dT\,d\Omega} = \frac{N_\pi(T)}{N_p\,N_t\,K} \qquad (1)$$

where $N_\pi(T)$ is the number of pions/cm^2 Mev entering the front face of the absorber, N_p is the number of protons passing through the target, N_t is the number of carbon nuclei or CH_2 molecules per cm^2, and K is a constant geometrical factor. Since the geometry was the same for all exposures, we only need to know the three quantities $N_\pi(T)$, N_p and N_t at the various pion energies in order to find the relative values of the cross sections.

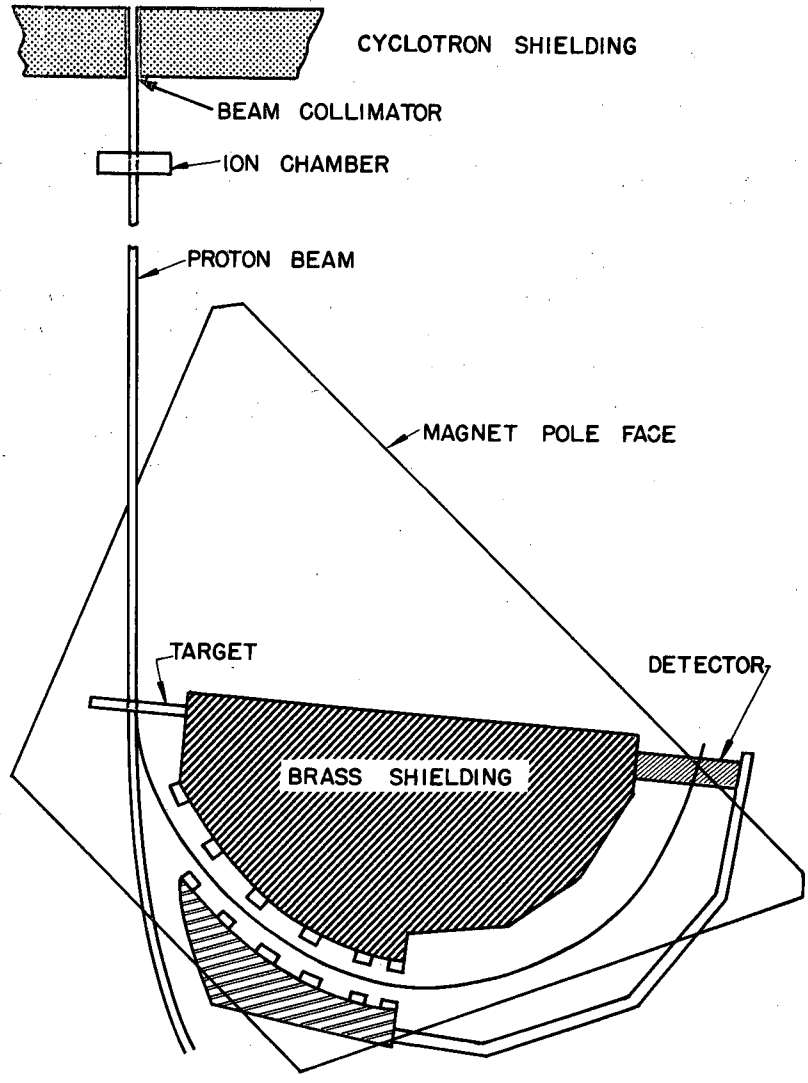

Fig. 1 Arrangement of experimental apparatus.

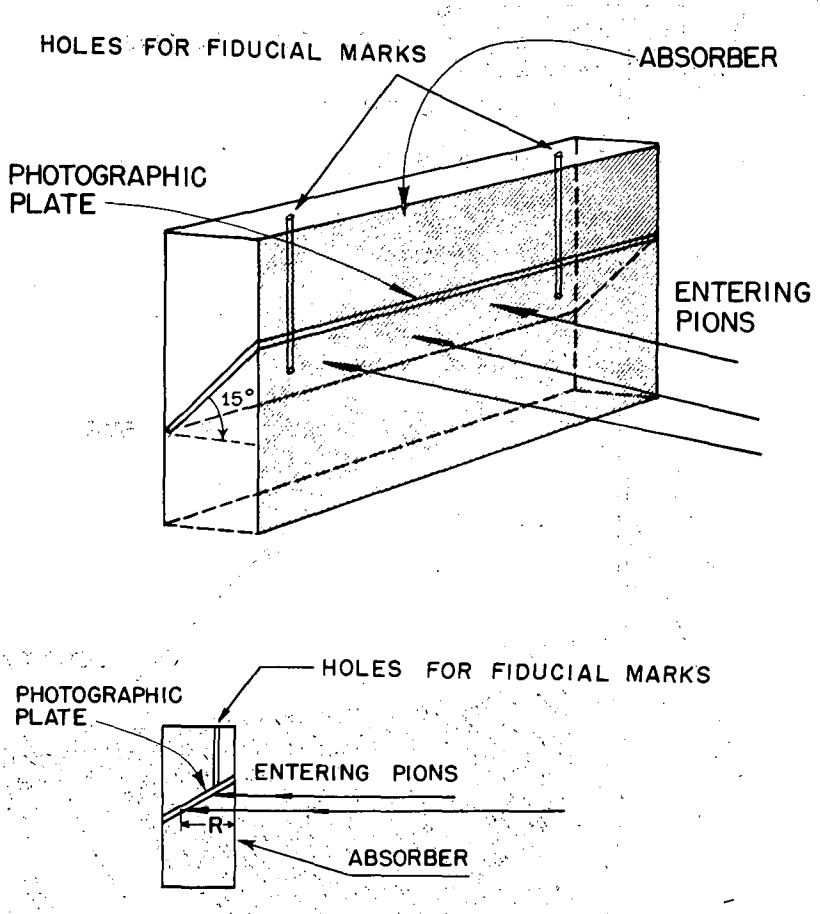

Fig. 2 Absorber blocks with photographic emulsions.

Four separate exposures were made: one each centered at 18.8, 21.7 and 24.8 Mev, using the CH_2 target, and one centered at 23.3 Mev using the carbon target. The magnetic field was changed to the appropriate value for each exposure, since the energy acceptance of the channel is too small (about 5 Mev) to cover the entire energy interval in one setting.

The energy of the incident proton beam was measured by determining the range of the protons in accurately machined copper absorbers. A Bragg curve was obtained by changing the thickness of the absorber interposed between two ion chambers. When the range-energy relation of Mather and Segrè[4] was applied to this curve, the energy of the incident proton beam was found to be 339 Mev. Taking this value for the proton energy and a pion mass of 273 electron masses,[5] we find that the pion produced at 0^o with an energy of 21.5 Mev has the same velocity as the neutron leaving the target at 0^o. This corresponds to a pion energy of 1.3 Mev and a neutron energy of 8.6 Mev in the center-of-mass system of the two initial nucleons.

The relative number of protons passing through the target during each exposure was determined by placing an ion chamber in the beam and integrating the output of the chamber.

In addition to these measurements of the relative production cross section, one measurement of the absolute production cross section was made at 21.7 Mev, using the CH_2 target. This measurement, though not so accurate as the relative measurements, was made for comparison with other data[3] and thus to insure that there was no "broad peak" present that would be missed in the relative measurements.

III DETAILS OF THE EXPERIMENTAL PROCEDURE

A. Target

We shall first show that a combination of requirements makes the use of a pure hydrogen target, either liquid or gaseous, impracticable.

The high rate of energy loss of a 20-Mev pion (about 5 Mev/g/cm^2) and the requirement for good energy resolution limits us to very thin targets. This would then lead to a high "background" of pions produced in the container walls of any such target. In order to calculate the solid angle, the point of origin of the pions should be fairly well localized and it should be either inside or very close to the edge of the magnetic field. This would introduce mechanical difficulties in the construction of a target.

It was thus decided to use polyethylene $(CH_2)_n$ and carbon to obtain the hydrogen contribution by subtraction.

The targets were mounted inside the magnetic field (see Fig. 1) and had the following approximate thicknesses:

$$CH_2 = 1/8 \text{ inch}$$
$$C = 1/4 \text{ inch}$$

The exact thicknesses were obtained by machining a portion of the target and weighing it accurately. The accurate values thus ascertained are:

$$CH_2 = 0.284 \text{ g/cm}^2$$
$$C = 0.991 \text{ g/cm}^2$$

The effective area of the target is the cross sectional area of the proton beam. The beam emerges from the cyclotron shielding through a 40-inch brass tube having a rectangular cross section of 1-1/4 inches high by 3/4 inch wide. At the target position, the beam has a rectangular cross section of approximately 1-3/4 inches high by 1-1/4 inches wide.

The energy loss of pions in traversing the entire target thickness is about 1.6 Mev for the CH_2 target and 4.8 Mev for the C target. The corresponding figures for the proton beam are about 1 Mev and 3 Mev.

B. Magnetic Field

The magnetic field used to separate the pion and proton trajectories has a maximum strength of 14,300 gauss across a 3-1/2 inch gap. The area of the pole face is large enough to permit a semicircular trajectory of about 10 inches radius within the uniform portion of the field. A measurement was undertaken along the central pion trajectory with a radius of 9.50 inches. A flip coil, which had previously been calibrated with a nuclear induction apparatus, was used for this purpose. A measurement of the relative field strength was made along the entire trajectory for a fixed value of the magnet current; an absolute measurement of the field strength as a function of magnet current was made at the target and detector position.

The field was found to be uniform within 1 percent over most of the trajectory. Over the last two inches there was a slight drop (up to 5 percent) owing to the fringing field.

The channel (see Section III, C) limits the trajectories reaching the detector to those within $\pm 4^{\circ}$ of the central trajectory. Since we are only concerned with a narrow pencil of trajectories, we make use of the following well-known focusing properties of uniform magnetic fields. Consider pions of a given energy leaving the target in a horizontal plane and with a small spread of angles around 0°. All the pions originating at a point in the target will, after turning through 180°, be focused to an image point at the detector. This will be true to a good approximation if we neglect the multiple small-angle scattering within the absorber. In this way all the pions of a given energy that can get down the channel will form a point-by-point image of the target on the photographic emulsion. The emulsions are then scanned in narrow swaths, each of which corresponds to a fixed value of the pion energy. The entire length of the target image is covered, and essentially all pions produced in a given energy interval and falling within the acceptance angle of the channel are thus detected.

C. Channel

The purpose of the brass channel is threefold:

(1) It serves as shielding for the detector by preventing particles that leave the target at angles other than 0° from reaching the emulsion.

(2) It defines the angular acceptance of the detector by a "slit" 1-1/4 inches wide at the 90° position. This limits the trajectories from the center of the target to $\pm 4^{\circ}$ with respect to the direction of the proton beam.

(3) It provides a rough energy selection by accepting only trajectories with the correct curvature. The energy "bite" δT of the channel is broader than the energy interval ΔT actually observed at the detector. At 22 Mev the energy bite of the channel is about 5 Mev.

The inside of the channel has a series of teeth protruding about 1/8 inch from the smooth wall of the channel. These teeth are about 1/4 inch thick and their purpose is to prevent reflections of particles from the metal walls. Such reflections ordinarily take place when a particle impinges on a smooth surface at a very small angle. The particle may then suffer a few scatters in the material and emerge again with a slightly different energy and direction of motion.

A wide acceptance angle for pions would be desirable since it leads to an increase in the solid-angle factor. We shall, however, show that such a wide acceptance angle is incompatible with the requirement of good energy resolution. It what follows we shall abbreviate the Center-of-Mass System of the two initial protons to "CM" and the Laboratory System to "Lab." Primed quantities are in the CM, unprimed quantities in the Lab. system. For a fixed pion energy in the CM, the energy in the Lab. is a rapidly varying function of the angle of emission in the CM.

$$T_{\pi}(\theta') = a + b \cos \theta'$$

where θ' is the angle of emission in the CM system;

T_π = kinetic energy of pion in Lab. system. For $\theta' = 45^\circ$, which corresponds to $\theta = 10^\circ$ in the Lab., for example, the energy drops from 21.5 to 19 Mev. It is thus necessary to limit the angular acceptance to a small value to avoid a large energy spread. The value chosen ($\theta = 4^\circ$ or $\theta' = 17^\circ$) corresponds to a drop of 0.4 Mev in pion energy.

The slit defining the angular acceptance of the channel is wide enough to permit each energy within ΔT to form a complete image of the target at the detector. This is necessary to assure the same effective target area for each energy within ΔT.

The cross sectional area of the pion beam was everywhere much larger than the RMS displacement, owing to multiple Coulomb scattering experienced by the pion in coming to rest in the absorber. For a 22 Mev pion, for example, the RMS displacement is 0.5 mm whereas the cross sectional area of the channel is nowhere less than 9 cm by 3 cm.

D. Geometry

Two different types of measurements were undertaken in this experiment, each using a different geometry.

The first type was a measurement of the relative production cross section. Here the pions were bent through 180° in the magnetic field. In order to calculate an absolute value of the cross section one needs to know, at a point in the target, the solid angle subtended by a unit area at the emulsion (perpendicular to the direction of travel of the pions). The reason for using this geometry is a very substantial reduction in the number of background tracks observed. Its main disadvantage lies in the complexity of the solid-angle calculation. The solid angle factor, however, does not enter into the determination of the relative cross section. In going from one energy to the next only the magnetic field is changed, and hence the geometry remains constant. An estimate of this factor was made, however, both by calculation and experimentally, and it was found to be close to the value in the 90° case (see below).

The second type was a measurement of the absolute production cross section. Since the above measurement gives information only

about the shape of the spectrum, it seemed advisable to check the absolute magnitude at one point. In this case the pions were only bent through 90° and the solid angle can be readily calculated. For pion trajectories perpendicular to the uniform magnetic field the solid angle is given[6] by

$$\frac{d\Omega}{dA} = \frac{1}{\rho^2 \phi \sin \phi} \text{ sterad/cm}^2 \qquad (2)$$

where ρ is the constant radius of curvature of the pion and ϕ is the angle through which the trajectory turns in going from the target to the absorber. For our case $\frac{d\Omega}{dA} = 1.1 \times 10^{-3}$ sterad/cm^2. This is for the trajectory from the center of target to the center of the absorber. The total variation in the solid angle for pions leaving different parts of the target and hitting the extreme edges of the detector is about 8 percent.

E. Detector

The detector consists of a photographic emulsion embedded in an aluminum absorber as shown in Fig. 2. Pions enter perpendicularly through the front face of the absorber and come to rest after having traveled a distance R equal to their range in aluminum. This range is 1 cm of aluminum for a 21-Mev pion. The population of stopped pions in the absorber is then sampled by the photographic emulsion. The energy of the pions coming to rest in the emulsion can thus be directly determined by their position on the emulsion and the known range-energy relation for pions in aluminum.[11] Fiducial marks were placed on the emulsions by shining light through two very small holes drilled at a known distance from the front face of the absorber. The depth of penetration into the absorber was then determined by the distance of the ending of the pion track from these fiducial marks.

We next have to establish a relation between the number of pions found per unit volume of emulsion and the flux of pions incident on the front face of the absorber. In Appendix 1 the following formula is derived.

$$N_\pi (T) = \frac{\rho_\pi}{\left[\frac{dT}{dx}\right]_{abs} \frac{R_{abs}}{R_{em}}} \qquad (3)$$

where $N_\pi (T)$ = No. of pions/cm^2 Mev entering the front face of the absorber.

ρ_π = pions stopped per unit volume of emulsion

$\frac{R_{abs}}{R_{em}} = \frac{\text{residual range in absorber}}{\text{residual range in emulsion}}$ at absorber-emulsion boundary

$\left[\frac{dT}{dx}\right]_{abs}$ = rate of energy loss when pion enters absorber.

The quantity ρ_π is experimentally observed and $N_\pi (T)$ is the quantity needed to calculate the cross section (see section III, H).

The above formula was derived on the assumption that the pion experiences no scattering as it penetrates through the absorber. However, the emulsion is embedded in an absorber of essentially infinite size compared to the RMS displacement due to scattering (see Sec. III, C). Hence to a good approximation the number of pions scattered out of any small volume of emulsion is compensated for by other pions (of slightly lower or higher energy) scattered into the emulsion from the surrounding absorber.

It is possible for protons having the same momentum as the pions of interest to come down the channel and enter the front face of the absorber block. However, the range of such protons is shorter by about a factor of 100, and hence such protons do not reach the emulsion.

F. Photographic Emulsions

The emulsions were scanned using a microscope with a magnification of 540 x. The only events counted were the ones in which the track could definitely be identified as that of a positive pion coming to rest. Such tracks could be recognized easily by the rapid variation of grain density and the large amount of scattering near the end of the range. The positive pion was further identified by the muon into which it decayed. The scanning efficiency was checked by letting different observers scan the same area in the emulsion. A series of such checks was made during the course of the experiment and the average scanning efficiency was found to be around 90 percent.

With the detector in the 180° position, the area scanned was a parallelogram in shape, to allow for the change of radius of curvature with energy (see Fig. 3). In this way the swath scanned for each individual energy is centered around its central trajectory, and the entire width of the target is thus covered. The area scanned was about 40 mm x 1.8 mm and was scanned in 12 swaths each 150 μ wide. Since the variation of energy along the plate is given (see App. 1) by

$$\Delta T = \left[\frac{d T}{d x}\right]_{abs} \Delta X = \left[\frac{d T}{d x}\right]_{abs} \cos \alpha \, \Delta S \qquad (4)$$

we find that $\Delta T = 12.5$ Mev/cm x 0.966 x 0.18 cm = 2.2 Mev. Hence the energy bite ΔT was about 2 Mev on each plate.

The thickness of the plates was determined by measuring the thickness of the glass plus emulsion immediately before exposure. After development, the same quantity was measured so as to give directly the shrinkage Δt of the emulsion. The dried emulsion was then measured on a calibrated microscope to get its final thickness t_f. The original thickness is thus obtained by adding the amount of shrinkage to the final thickness of the emulsion, i.e. $t_f + \Delta t$.

G. Measurement of Proton Beam Energy

The energy of the electrically deflected proton beam was measured by a method originally used by Bakker and Segrè[7]. The beam first passes through a thin ionization chamber filled with argon at about atmospheric pressure. It then passes through a set of accurately machined and weighed copper absorbers of variable thickness and finally through a second ionization chamber similar to the first one. The distance between the collecting foils in each chamber is 2 inches and their diameter is large enough (4 inches) to allow for the broadening of the beam due to multiple scattering in the absorber.

The charge collected in each chamber is integrated and the ratio of the outputs of the two chambers is recorded. A plot of this ratio as a function of absorber thickness yields the well-known Bragg curve.

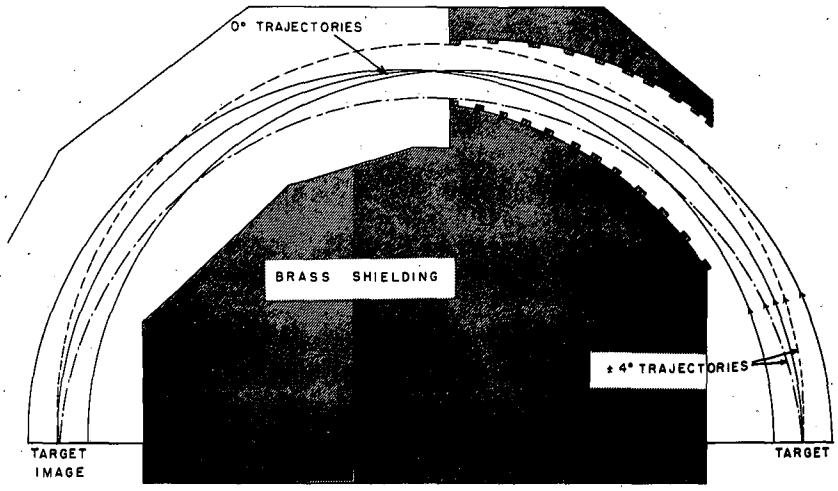

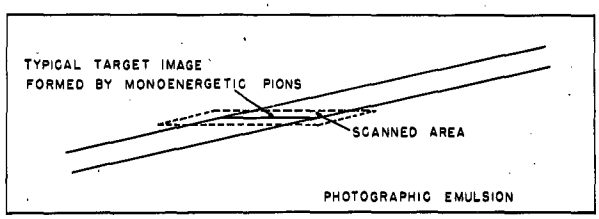

Fig. 3 Pion trajectories in magnetic field and target images formed on photographic emulsion.

Mather and Segrè[4] have shown that if one chooses on this curve a value of the ordinate which is 0.82 times the maximum value, one obtains at the corresponding abscissa the "range" of the particle.

The proton beam energy was measured, using the above criterion for the range and the values for the range in Cu quoted by the same authors.

Four separate measurements of the beam energy were undertaken, yielding the following values:

Date	Range in Cu (g/cm^2)	Energy in Mev
July 8, 1952	92.1	339.4
July 9, 1952	92.2	339.4
Sept. 20, 1952	91.3	338.1
Sept. 21, 1952	91.4	338.2

From the shape of the Bragg curve we can also obtain an estimate of the energy spread in the proton beam. The spread is of the order of ± 2 Mev and since the pion energy T_π is a fairly slowly varying function of the incident-beam energy this will not introduce a large shift in pion energies. A change in proton energy of 1 Mev will cause a change in pion energy of 0.15 Mev. Thus the uncertainty in pion energies due to the inhomogeneity of the proton beam is considerably smaller than the energy spread due to the finite target thickness (~ 0.8 Mev).

H. Calculation of Cross Section

Here again we have to distinguish between the two types of measurements made, one to obtain the relative cross section and the other to obtain the absolute value. In general, the number of pions entering the face of the absorber per unit area per Mev is related to the cross section as follows:

$$N_\pi (T) = N_p N_t \left(\frac{d\sigma}{dT\, d\Omega}\right)\left(\frac{d\Omega}{dA}\right), \qquad (5)$$

where $N_\pi (T)$ = Number of pions entering absorber face/cm^2 Mev

N_p = Number of protons passing through target

N_t = Number of carbon nuclei or CH_2 molecules in target/cm^2

$\frac{d\sigma}{d\Omega\, dT}$ = Differential cross section for production of pions by protons on carbon nuclei (or a CH_2 group) per unit solid angle per Mev.

$\frac{d\Omega}{dA}$ = Solid angle subtended by a unit area at the emulsion.

The number of protons N_p was determined by integrating the output of a calibrated ion chamber placed in the beam just ahead of the target. The number of target nuclei is also easily determined from the known thicknesses of the targets.

Consider now the case where the detector is placed in the 180° position and we want to measure the relative production cross section. A given unit area on the absorber face can be reached by pions from all parts of the target. See Fig. 3 for a set of typical trajectories. Each point of the target contributes pions of a different energy to the same unit area on the absorber face. Assuming that the density of protons striking the target is uniform within the area of the beam, we are justified in using Eq. (5) above, which was derived on the assumption of uniform contributions from all parts of the target within the energy interval chosen. The factor $\frac{d\Omega}{dA}$ remains a constant as the magnetic field is changed and thus does not enter into the determination of the relative cross section.

With the detector in the 90° position, the conditions for use of Eq. (5) are satisfied, since now pions can reach the element dA on the absorber face by leaving the target at a small angle to the beam direction. Thus here, too, pions within the energy acceptance of the channel can reach any part of the detector from any part of the target.

If we now use the expression for $N_\pi(T)$ from Eq. (3) above we get

$$N_\pi(T) = \frac{\rho_\pi}{\left[\frac{dT}{dx}\right]_{abs} \frac{R_{abs}}{R_{em}}} = N_p\, N_t \left(\frac{d\sigma}{d\,T\, d\,\Omega}\right)\left(\frac{d\,\Omega}{dA}\right) \qquad (6)$$

or

$$\frac{d\sigma}{dT\,d\Omega} = \frac{\rho_\pi}{\left[\frac{dT}{dx}\right]_{abs} \frac{R_{abs}}{R_{em}} N_p N_t \frac{d\Omega}{dA}} \text{ cm}^2/\text{sterad. Mev} \quad (7)$$

I. Corrections to Cross Section

The above value for the cross section has to be corrected for two effects that tend to remove pions from the beam before the emulsion is reached. These effects are:

(1) Decay of pions in flight

(2) Nuclear interactions while slowing down in the absorber.

As is shown in Appendix 2, both these corrections are very slowly varying functions of the pion energy and hence do not have to be included in the evaluation of the relative cross section. The third correction is applicable to both relative and absolute cross sections, and takes into account the finite thickness of the target.

(1) Correction for pion decay in flight.

Because the pion has a fairly short mean life($\tau_m = 2.54 \times 10^{-8}$ sec),[8] an appreciable fraction of the pions leaving the target decay before they reach the emulsion. The time elapsed (in the pion's frame of reference) is the time of flight in air τ_{air} plus the time it takes the pion to come to rest after entering the absorber τ_{abs}. In Appendix 2 the following expression is derived for the total elapsed time τ_t

$$\tau_t = \tau_{air} + \tau_{abs} = 3.3 \times 10^{-11} \sqrt{\frac{Mc^2}{2T}} \left(\frac{\rho\phi}{\sqrt{1 + T/2Mc^2}}\right)$$

$$+ 4.70 \times 10^{-11} \sqrt{\frac{Mc^2}{2T}}\, R \text{ (insec.)} \quad (8)$$

where ρ = radius of curvature of pion in magnetic field

ϕ = angle through which trajectory turns

T = kinetic energy (in Mev)

Mc^2 = rest mass of pion (in Mev)

R = range of pion in absorber (in cm)

Hence the observed cross section σ_{obs} equals the corrected cross section σ_{corr} times the fraction of pions that survived in transit.

$$\text{Thus: } \sigma_{obs} = \sigma_{corr}\, e^{-\frac{\tau_t}{\tau_m}} \qquad \text{or}$$

$$k_d = \frac{\sigma_{corr}}{\sigma_{obs}} = e^{\frac{\tau_t}{2.54 \times 10^{-8}}} \tag{8}$$

This correction is of the order of 10 percent for the energies and geometry in this experiment.

(2) Correction for nuclear interactions in the absorber.

Nuclear interactions in the absorber also decrease the flux of pions reaching the emulsion. Although the cross section for such nuclear events has been measured recently for a number of elements and several energies,[9] the information available is still insufficient for an accurate correction. The available data do, however, indicate that the assumption of nuclear area for the combined absorption and large-angle scattering cross sections is a fairly good one. Hence we take πr^2 as the attenuation cross section, where $r = 1.4 \times 10^{-13} \times A^{1/3}$ cm. The number of nuclei per cm^2 is given by $\frac{q R A_o}{A}$ where

q = Density of absorber material in g/cm^3

R = Range in the absorber (in cm)

A_o = Avogadro's number

A = Atomic weight of absorber material.

We thus have again: $\sigma_{obs} = \sigma_{corr}\, e^{-\frac{\sigma q R A_o}{A}}$ or

$$k_{abs} = \frac{\sigma_{corr}}{\sigma_{obs}} = e^{\frac{\sigma q R A_o}{A}} \tag{9}$$

At 20 Mev pion energy this correction is of the order of only 2 percent.

(3) Correction for thick target.

The quantity measured in this experiment is the number of pions of kinetic energy T produced in an energy interval Δ T. The pions emerging from the target in the energy interval Δ T at energy

T have been produced at various depths in the target, with an energy $T' = T + \left(\frac{dT}{dx}\right)t$ where $\left(\frac{dT}{dx}\right)$ is the energy loss per centimeter of a pion of energy T and t is the target thickness between the piont of production and its exit from the target.

For two low-energy pions of slightly different energy, there is an appreciable difference in the rate of change of the specific ionization as we go from the front of the target to the back. Hence pions produced in an energy interval $\Delta T'$ will emerge from the target spread over an energy interval ΔT. In Appendix 2 it is shown that these two energy intervals are related as follows:

$$\Delta T = \Delta T' \frac{\left(\frac{dT}{dx}\right)_T}{\left(\frac{dT}{dx}\right)_{T'}}$$

Since the energy interval used in calculating the differential cross section is ΔT rather than the actual $\Delta T'$, we must multiply the answer by

$$k_{th} = \frac{\Delta T}{\Delta T'} = \frac{\left(\frac{dT}{dx}\right)_{Exit}}{\left(\frac{dT}{dx}\right)_{T'}} \qquad \text{where } \left(\frac{dT}{dx}\right)_{T'} \qquad (11)$$

has been averaged over the target. The magnitude of this correction is about 10 percent.

IV EXPERIMENTAL RESULTS

The experimental results are listed in Table I. The normalized values shown in column 7 were obtained by making the relative measurement of the CH_2 cross section at 21.7 Mev agree with the absolute value measured at that point. The errors listed in Table I are statistical probable errors with the exception of the energy spreads in column 3. The uncertainties in the energy are due to the finite thickness of the target. For purposes of comparison the data obtained by W. F. Cartwright et. al.[3] have also been listed in Table I.

In Table II the values for the hydrogen cross section are shown as obtained by subtraction of the CH_2 and C cross sections. In making the subtraction a small correction was applied to the value of the C cross section to allow for the shape of the carbon spectrum. The slope of the curve was obtained from the work of W. Dudziak[10].

The absolute value of the cross section is assigned a 15-percent error because of the uncertainties in the scanning efficiency of the observer, the beam integration equipment, the measurement of the plate thickness, etc. The 15-percent error was assigned on the basis of the following estimates of the accuracy of the major factors:

Error in the number of pions counted	10%
Error in measurement of original emulsion thickness	8%
Error due to averaging of solid angle	5%
Error in beam integration	5%

Fig. 4 shows a graph of the experimental data.

Table I

Differential cross section for production of positive pions by 340 Mev protons on CH_2 and carbon

Column 1	2	3	4	5	6	7
Type of measurement	Target	Pion energy Mev	No. of pions found	Uncorrected cross section	Corrected cross section	Normalized value of cross section cm^2/sterad Mev
Relative	CH_2	18.8 ± 1.2	103	1.03	1.08 ± 0.07	$3.9 \pm 0.25 \times 10^{-30}$
Relative	CH_2	21.7 ± 1.1	107	1.30	1.34 ± 0.09	$4.8 \pm 0.32 \times 10^{-30}$
Relative	CH_2	24.8 ± 1.1	85	1.08	1.16 ± 0.08	$4.2 \pm 0.29 \times 10^{-30}$
Relative	C	23.2 ± 2.4	175	0.85	0.92 ± 0.05	$3.3 \pm 0.18 \times 10^{-30}$
Absolute	CH_2	21.7 ± 1.1	58	4.1×10^{-30}	$4.8 \pm 0.42 \times 10^{-30}$	----
Absolute*	CH_2	17.5		3.0×10^{-30}	$3.8 \pm 0.6 \times 10^{-30}$	----
Absolute*	C	17.5		1.9×10^{-30}	$2.5 \pm 0.3 \times 10^{-30}$	----
Absolute*	CH_2	34.0		5.3×10^{-30}	$6.7 \pm 0.7 \times 10^{-30}$	----
Absolute*	C	34.0		3.3×10^{-30}	$4.3 \pm 0.4 \times 10^{-30}$	----

*Data of W. F. Cartwright et. al. (see reference 3)

In columns 5 and 6 the relative cross sections are in arbitrary units, the absolute cross sections are in cm^2/sterad Mev

Table II

Differential cross section for production of positive pions by 340-Mev protons on protons

Pion Energy (Mev)	σ_{CH_2} Arbitrary units	σ_C Arbitrary units	σ_H Arbitrary units	Normalized value of σ_H cm^2/sterad Mev
18.8	1.08 ± 0.07	0.84 ± 0.05	0.12 ± 0.04	$0.4 \pm 0.1 \times 10^{-30}$
21.7	1.34 ± 0.09	0.88 ± 0.05	0.23 ± 0.05	$0.8 \pm 0.2 \times 10^{-30}$
24.8	1.16 ± 0.08	0.96 ± 0.05	0.10 ± 0.05	$0.4 \pm 0.2 \times 10^{-30}$
17.5*				$0.6 \pm 0.3 \times 10^{-30}$
34.0*				$1.2 \pm 0.4 \times 10^{-30}$

*Data of W. F. Cartwright et. al. (see reference 3)

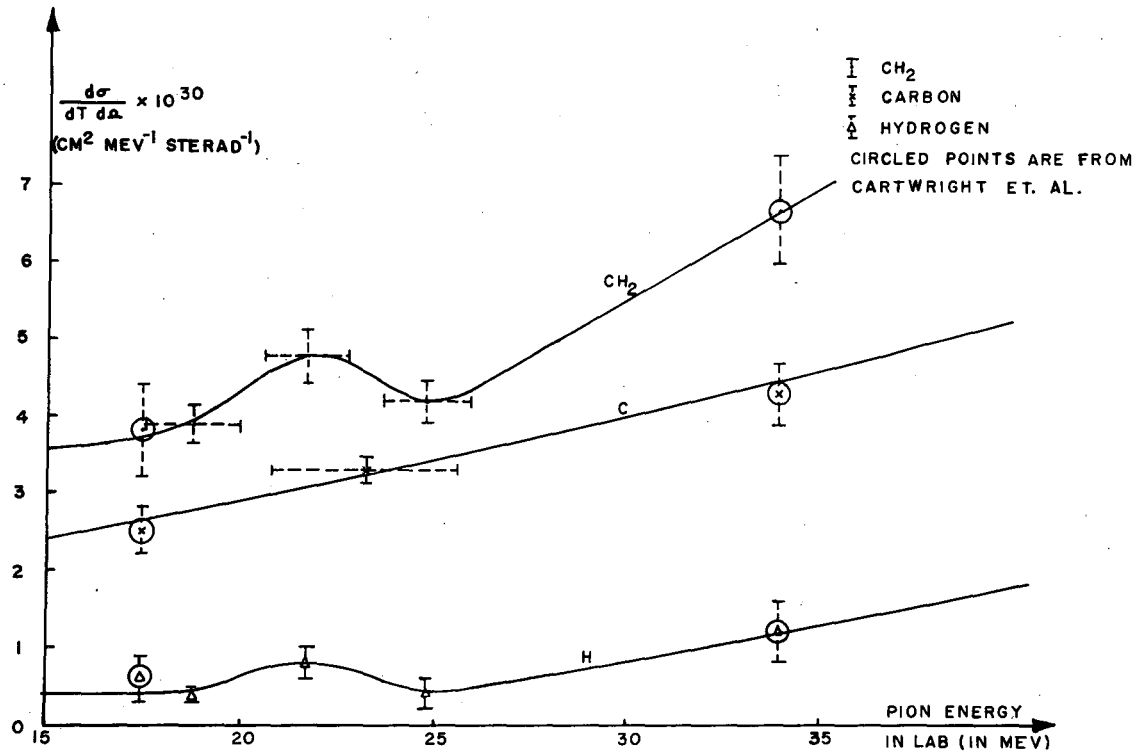

Fig. 4 Experimental results.

V DISCUSSION

A. Discussion of Experimental Results

Because of the small difference between the CH_2 and carbon spectra, the values for the hydrogen cross section have very large statistical errors, which make the interpretation of the results rather speculative. The two extreme situations of either a very large increase in the cross section or a depression in the cross section can be excluded with reasonable certainty, however.

An inspection of the hydrogen curve shows that the point at 21.7 Mev is slightly higher than the other two points. In view of the statistical errors of these measurements, however, it is doubtful whether this peak represents a real effect.

That the points measured do not lie on a broad peak is clearly shown by comparison with the points of Cartwright et al.[3] on either side of the energy interval investigated.

Both these facts lead to the conclusion that there is at most a small departure from the flat and slowly rising shape of the hydrogen spectrum in the energy interval of 18 to 26 Mev.

B. Kinematics

As far as the kinematics of the reaction $p + p \rightarrow \pi^+ + p + n$ are concerned, there can be two different configurations of the final reaction products. Both the following cases are in the CM and, since the total kinetic energy shared by the three final particles is only 21.3 Mev, all calculations in the CM of these particles are carried out non-relativistically. All transformations from the Lab. system to the CM system and vice versa must of course be done relativistically.

Case A: No two of the final particles come off at the same angle.

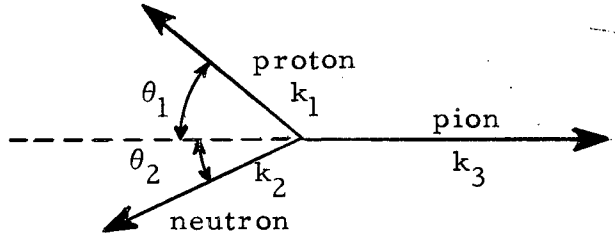

Fig. 5

Case B: The pion and one of the nucleons, say the neutron, come off together and in the forward direction. This case corresponds to $\theta_1 = 0^\circ$ and $\theta_2 = 180^\circ$.

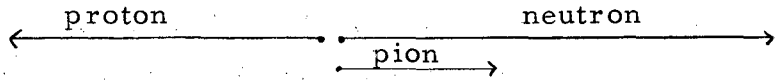

For either case A or case B the relevant quantity in the description of the pion-neutron system is the relative momentum of the pion and neutron, which is defined as follows:

$$\vec{K} = \frac{m_3 \vec{k}_2 - m_2 \vec{k}_3}{m_2 + m_3} \qquad (12)$$

where m_2 = neutron mass
k_2 = neutron momentum
m_3 = pion mass
k_3 = pion momentum

The relative energy T_{rel} is then given by

$$T_{rel} = \frac{K^2}{2\left(\frac{m_2 m_3}{m_2 + m_3}\right)} \qquad (13)$$

The relative momentum was calculated as a function of the pion momentum and hence of pion energy. From the conservation laws for energy and momentum we obtain an expression for k_2 as a function of k_3 which has the form

$$k_2 = c_1 k_3 \cos\theta_2 + \sqrt{k_3^2 (c_2 \cos^2\theta_2 + c_3) + c_4} \quad , \qquad (14)$$

where θ_2 is the angle of the neutron momentum as shown in Fig. 5 and the c's are constants which depend on the particle masses and the available energy T_A only.

Substitution of this expression in Eq. (12) gives the relative momentum K as a function of the pion momentum and the neutron angle θ_2.

Now let us consider case B, which is the special case of $\theta_2 = 180^\circ$ or $\cos \theta_2 = -1$. The expression for k_2 then reduces to

$$k_2 = - c_1 k_3 + \sqrt{k_3^2 (c_3 + c_2) + c_4} \qquad (15)$$

and the corresponding expression for the relative momentum K then becomes

$$K = \sqrt{c_5 k_3^2 + c_6} - c_7 k_3 \qquad (16)$$

Table III shows the numerical values of the relative momentum K and the relative energy T_{rel} for various values of the pion momentum k_3. The corresponding curves are plotted in Fig. 6.

The factor f is a constant numerical factor, whose value is 3.817×10^{-17}.

If, in Eq. (16) above, we set the relative momentum K equal to zero and solve for k_3, we obtain the pion momentum for which the condition of zero relative velocity holds. This critical value of the pion momentum is

$$k_3 = 26.44 \text{ f } \left(\frac{\text{g cm}}{\text{sec}}\right)$$

corresponding to a pion energy in the CM of 1.28 Mev. In the Lab. this pion has an energy of 21.5 Mev.

We now return to case A and consider the variation of the neutron momentum k_2 with neutron angle θ_2, keeping the pion momentum fixed in magnitude and direction (see Fig. 5). A series of values for the neutron momenta was calculated keeping the pion momentum fixed at 180° and a magnitude of 26.488 f $\frac{\text{g} \cdot \text{cm}}{\text{sec}}$. These values are shown in Table IV.

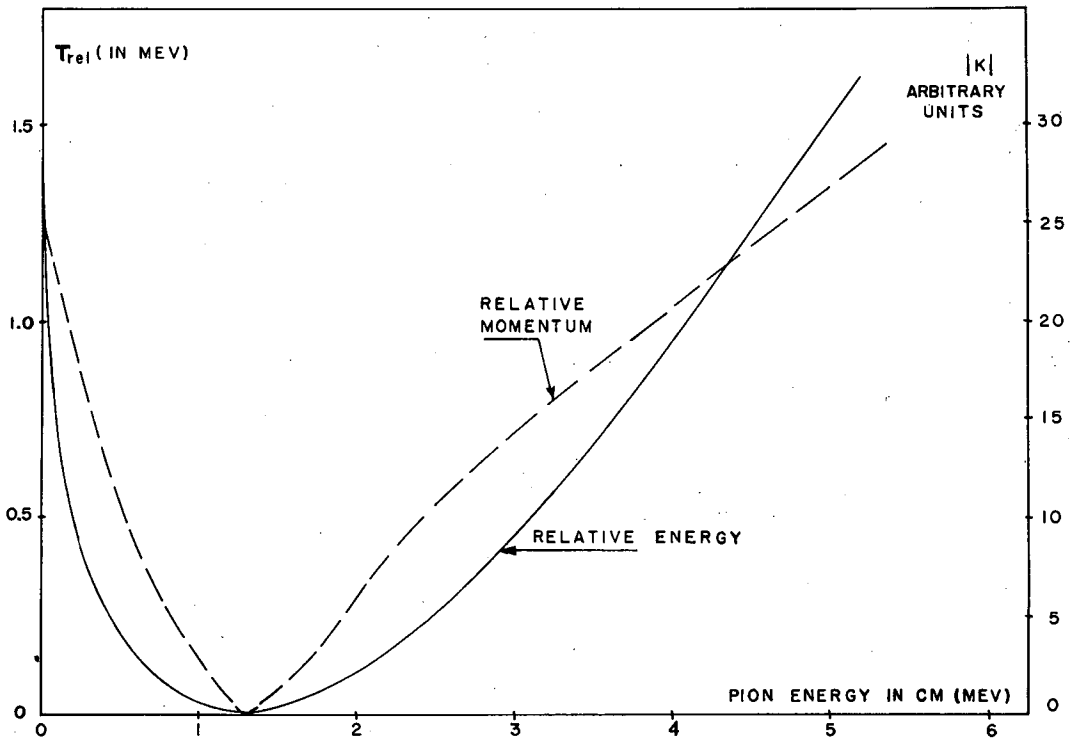

Fig. 6 Relative pion-neutron energy and momentum as a function of pion energy in the CM system.

Table III

Pion Energy in Lab. $T_{\pi_{lab}}$ (in Mev)	12.04	18.99	21.47	25.96	33.32
Pion energy (in CM) T_{π} (in Mev)	0	0.75	1.28	2.50	5.00
Pion momentum (in CM) k_3 (in $\frac{g\cdot cm}{sec}$)	0	20.24f	26.49f	36.95f	52.50f
Relative momentum K (in $\frac{g\cdot cm}{sec}$)	25.64f	6.15f	-0.06f	-10.66f	-26.77f
Relative energy T_{rel} (in Mev)	1.37	0.08	0.00	0.24	1.51
Relative velocity $v_2 - v_3$ (in $\frac{cm}{sec}$)	4.50×10^{9}	1.08×10^{9}	-0.01×10^{9}	-1.88×10^{9}	-4.72×10^{9}

Summary of Kinematical Quantities

Table IV

Relative Pion-Neutron Energy and Momentum as a Function of Angle of Neutron Emission (for fixed pion momentum).

Neutron angle θ (in CM)	Neutron momentum k_2 (in CM) (g cm/sec)	Relative momentum K (g cm/sec)	Relative energy T_{rel}
0^o	204.48f	49.44f	0.51 Mev
30^o	202.58f	47.30f	0.47 Mev
60^o	197.51f	41.82f	0.37 Mev
90^o	190.76f	33.72f	0.24 Mev
120^o	184.26f	23.39f	0.15 Mev
150^o	179.63f	11.92f	0.03 Mev
180^o	177.98f	0.06f	0.00 Mev

Since all of these neutron momenta are associated with the same pion momentum, there is no way to separate, experimentally, cases with different neutron angles as long as k_3 remains the same. As a consequence of this, we must associate a spread of relative momenta K with each value of pion momentum rather than just a single value.

This effect tends to smear out the peak in the production cross section, since the values of K associated with neighboring values of k_3 partially overlap. In the next section we analyze this effect in greater detail.

Finally, we want to look at the variation of the relative momentum K as the pion momentum changes from the central to the extreme position within the acceptance angle of the channel. The acceptance angle of the channel is $\pm 4^o$ in the Lab., which corresponds to $\pm 17^o$ in the CM. If we go back to case B and then let the pion momentum vary from 180^o to 163^o while keeping the neutron momentum fixed at 180^o, we find that K changes by only a small amount, namely from 0.06 f to 0.54 f. This variation in K is quite negligible compared to the variation in K due to the angle of neutron emission.

C. Interpretation of Experimental Results

By the use of the idea of a "scattering length" and a phenomenological description very similar to the one used in the analysis of low-energy n-p scattering, it is possible to derive an expression for the effect of the pion-nucleon interaction on the pion spectrum. In this section we first give an outline of the derivation of this formula and then discuss to what extent numerical values for the scattering length can be obtained by a comparison of the experimental and theoretical curves. In the derivation we consider only the pion-neutron interaction, although the proton is kinematically equivalent to the neutron. Thus if we neglect Coulomb effects the neutron may everywhere be replaced by the proton and we obtain the same results as before.

The following assumptions are made:

1) The pion-neutron interaction can be represented by an attractive well, whose depth is large compared to the relative pion-neutron energy
2) The matrix element for pion production can be considered constant over the energy region under investigation (0.5 to 2.5 Mev pion energy in the CM system)
3) The range of the interaction is short compared to the pion wave length. In addition it is assumed that the pion wave length is large compared to the distance between the nucleons during the pion-production process.

The theory shows that under these assumptions the form of the wave function inside the well is independent of the energy and we may thus write

$$\psi_{\pi}(K, r) = h(r)\, f(K) , \qquad (17)$$

where the entire energy dependence of the wave function is contained in $f(K)$, K being again the relative pion-neutron momentum. The function $h(r)$ will affect the magnitude of the cross section but not its energy dependence. Hence the energy spectrum will be obtained by integrating $|f(K)|^2$ over the phase space available to the reaction products.

For the wave function outside the well we have

$$f(K) \sim \frac{\sin(Kr + \delta)}{K} \quad , \tag{18}$$

and for small values of K r (K r << 1) we obtain the following approximate form for the pion wave function at the neutron:

$$\left|f(K)\right|^2 \sim \left|\frac{\sin \delta}{K}\right|^2 \quad . \tag{19}$$

The differential production cross section will then have the form

$$d\sigma = |M|^2 \left(\frac{\sin^2 \delta}{K^2}\right) \rho_T \tag{20}$$

where M = matrix element for pion production

ρ_T = density of final states.

It is easily shown from the boundary conditions at the edge of the well that the second factor in the above formula can be rewritten

$$\frac{\sin^2 \delta}{K^2} = \frac{1}{K^2 + a^2} \tag{21}$$

where K = relative pion-neutron momentum

$a = \frac{1}{a}$ and a = scattering length

In order to obtain the density of final states we specify our system by the following two vectors:

$\vec{k}_3$ = pion momentum

$\vec{g} = \frac{\vec{k}_1 - \vec{k}_2}{2}$ = the relative proton-neutron momentum

The vector $\vec{g}$ was chosen rather than $\vec{K}$ because the energy can be expressed as a simple function of $\vec{g}$ and $\vec{k}_3$ and these two vectors completely

specify the state of the system. The density of final states is then

$$\rho_T = k_3^2 \, dk_3 \, d\omega_3 \, g^2 \frac{dg}{dT} \, d\omega g \tag{22}$$

and substituting these expressions into equation (20) above we have for the differential cross section at a fixed value of θ the expression

$$\left.\frac{d\sigma}{dk_3 d\omega_3}\right|_\theta \sim \left(\frac{1}{K^2 + a^2}\right) k_3^2 \, g^2 \frac{dg}{dT} \, d(\cos\theta) \, . \tag{23}$$

Using the conservation laws for energy and momentum we obtain expressions for $\vec{K}$ and $\vec{g}$ as functions of the pion momentum $\vec{k}_3$

$$K^2 = \left(\frac{\mu}{\mu + M}\right)^2 \left[k_3\left(\frac{1}{2} + \frac{M}{\mu}\right) - g\right]^2 \tag{24}$$

$$g^2 = MT_A - k_3^2 \left(\frac{M}{2\mu} + \frac{1}{4}\right) \tag{25}$$

where M = nucleon mass

μ = pion mass

T_A = kinetic energy available in CM system

θ = angle between $-\vec{k}_3$ and $\vec{g}$ as shown in Fig. 7.

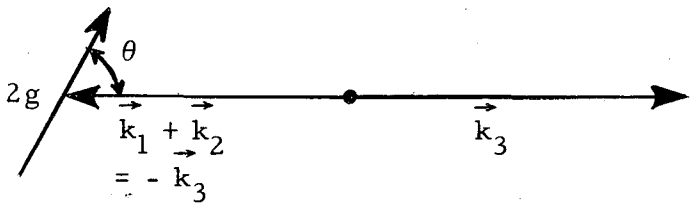

Fig. 7

We now integrate over all values of θ thus including all possible orientations of the neutron momentum k_2 for a fixed value of the pion momentum k_3. It is this process of averaging over all neutron momenta which tends to smear out the peak in the pion spectrum. We next substitute

the values for $\vec{K}$ and $\vec{g}$ into the cross section formula and thus obtain an integral of the form

$$\frac{d\sigma}{dk_3\, d\omega_3} \sim \int_{-1}^{1} \frac{k_3^2\, g\, d(\cos\theta)}{\left\{a^2 + \frac{1}{4}\left(\frac{\mu + 2M}{\mu + M}\right)^2 k_3^2 + \left(\frac{\mu}{\mu + M}\right)^2 g^2\right\} + \frac{\mu(\mu + 2M)}{(\mu + M)^2} k_3\, g \cos\theta} \tag{26}$$

which upon integration and substitution of the limits becomes

$$\frac{d\sigma}{dk_3\, d\omega_3} \sim k_3 \log \frac{a^2\left(1 + \frac{M}{\mu}\right)^2 + g^2 + \left(\frac{1}{2} + \frac{M}{\mu}\right)^2 k_3^2 + \left(1 + \frac{2M}{\mu}\right) k_3\, g}{a^2\left(1 + \frac{M}{\mu}\right)^2 + g^2 + \left(\frac{1}{2} + \frac{M}{\mu}\right)^2 k_3^2 - \left(1 + \frac{2M}{\mu}\right) k_3\, g} \tag{27}$$

Before we can compare this cross section with the experimental points we must change the independent interval from pion momentum to pion energy. This we do by noting that the total number of pions is given by

$$N = \frac{d\sigma}{dk_3\, d\omega_3}\, dk_3 = \frac{d\sigma}{dT_3\, d\omega_3}\, dT_3$$

and hence

$$\frac{d\sigma}{dT_3\, d\omega_3} = \frac{\mu}{k_3} \frac{d\sigma}{dk_3\, d\omega_3}$$

We thus have to divide the momentum spectrum by k_3 to obtain the energy spectrum which then has the final form

$$\frac{d\sigma}{dT\, d\omega} \sim \log \frac{a^2\left(1 + \frac{M}{\mu}\right)^2 + g^2 + \left(\frac{1}{2} + \frac{M}{\mu}\right)^2 k_3^2 + \left(1 + \frac{2M}{\mu}\right) k_3\, g}{a^2\left(1 + \frac{M}{\mu}\right)^2 + g^2 + \left(\frac{1}{2} + \frac{M}{\mu}\right)^2 k_3^2 - \left(1 + \frac{2M}{\mu}\right) k_3\, g} \tag{28}$$

In Fig. 8 is shown a series of curves each representing the shape of the cross section for a different value of a. The vertical scale is in aribtrary units since we are not interested in the absolute magnitude of the spectrum. Also plotted in the same figure are the experimental points for hydrogen and their probable errors as listed in Table II.

If one tries to deduce a minimum and maximum value for a, and hence for the scattering length, from a comparison of the data and the calculated curves one would be led to values of the following order of magnitude

Minimum	$a = 0.001 \left(\frac{\mu c}{\hbar}\right)$	$a = 1.5 \times 10^{-10}$ cm
Maximum	$a = 0.05 \left(\frac{\mu c}{\hbar}\right)$	$a = 3 \times 10^{-12}$ cm

Both of these values appear to be unreasonably large on the basis of other pion-scattering experiments and on the basis of theoretical estimates. Although no experiments have to date been performed at such low energies, the theoretical estimates seem to point to a scattering length of the order of 10^{-13} cm.

This discrepancy, as well as the wide range of scattering lengths that seem compatible with the data, is a consequence of the fact that the height of the peak is a rather insensitive function of a. As a final conclusion we may thus state that if an attractive pion-nucleon interaction does exist at these energies, its magnitude is not sufficiently large to be detected by an experiment of this type.

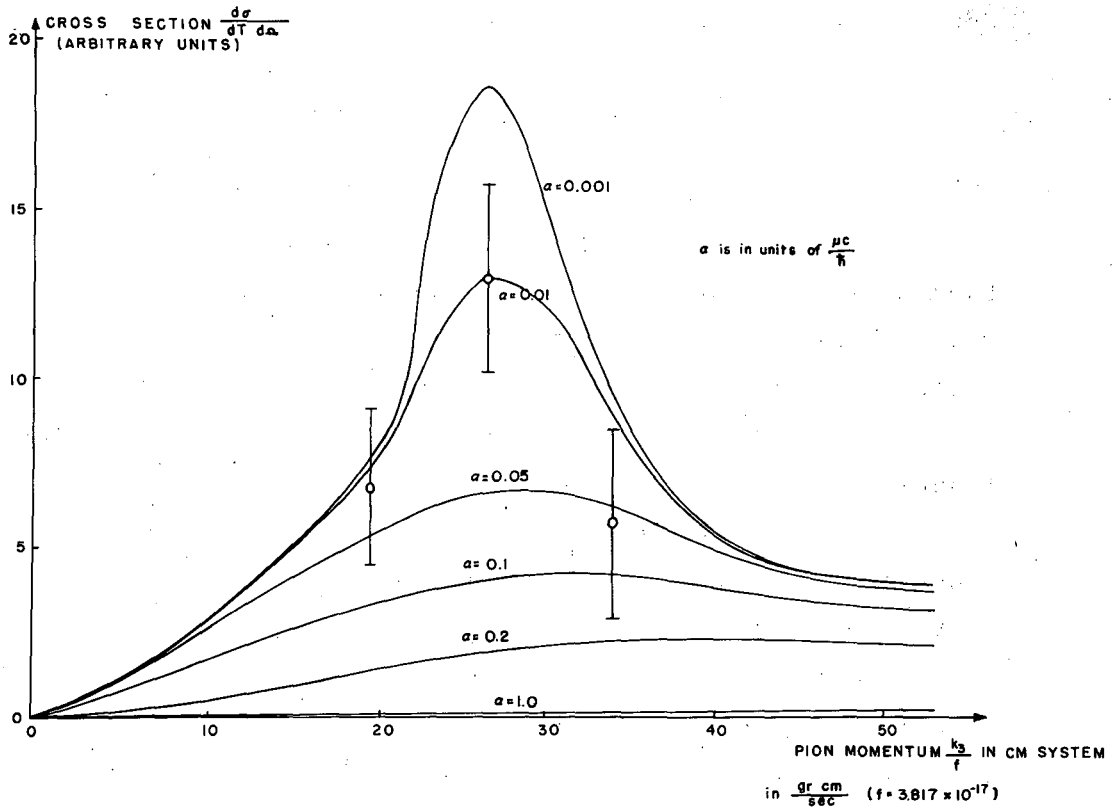

Fig. 8 Experimental points and calculated shape of cross section for various values of a.

VI ACKNOWLEDGEMENTS

The planning and execution of the experiment in its early stages were carried out together with Dr. W. F. Cartwright, who contributed greatly at all stages to the work.

I wish to express my gratitude to Prof. C. Richman for his guidance and encouragement during the course of the experiment. I am especially indebted to Dr. M. N. Whitehead for many helpful suggestions and to Dr. S. Tamor for making available to me his unpublished work on the theoretical aspects of this problem.

I also wish to thank Mrs. B. Baldridge and Miss. I. d'Arche for their help in the scanning of the emulsions.

VII APPENDIX

1. Derivation of the Detection Efficiency of the Photographic Emulsion

The relationship between the number of pions incident on the detector and the density of pions actually observed in the photographic emulsion is a measure of the efficiency of the detector. By the detector is meant the aluminum absorber block with the emulsion embedded in it. Let us for the moment assume no scattering inside the detector.

Consider a uniform flux of monoenergetic pions of energy T incident on the detector as shown in Fig. 9. These pions have a range R(T) in the material of the absorber given by the range-energy relation.[11] However, only those pions whose trajectories fall within the band of width "a" shown in Fig. 9 stop in the emulsion and are detected, while all other pions come to rest in the absorber.

If the thickness of the emulsion is d and the angle of inclination to the horizontal α, we have

$$\tan \alpha = \frac{a}{R_{abs}} \quad \text{and} \quad \sin \alpha = \frac{d}{R_{em}}$$

where R_{abs} and R_{em} are the residual ranges in the absorber material and the emulsion respectively at the point shown. At this point the pions have an energy T_{res}, which in our case is about 5.4 Mev. Dividing one expression for α by the other yields

$$\frac{\tan \alpha}{\sin \alpha} = \frac{a\, R_{em}}{d\, R_{abs}} \quad \text{or}$$

$$a = d \sec \alpha \frac{R_{abs}}{R_{em}} \tag{29}$$

Next let us consider a beam of pions with a small spread of energies ΔT around T. The number of pions coming to rest in a strip of emulsion of length ℓ (perpendicular to the paper in Fig. 9) is then

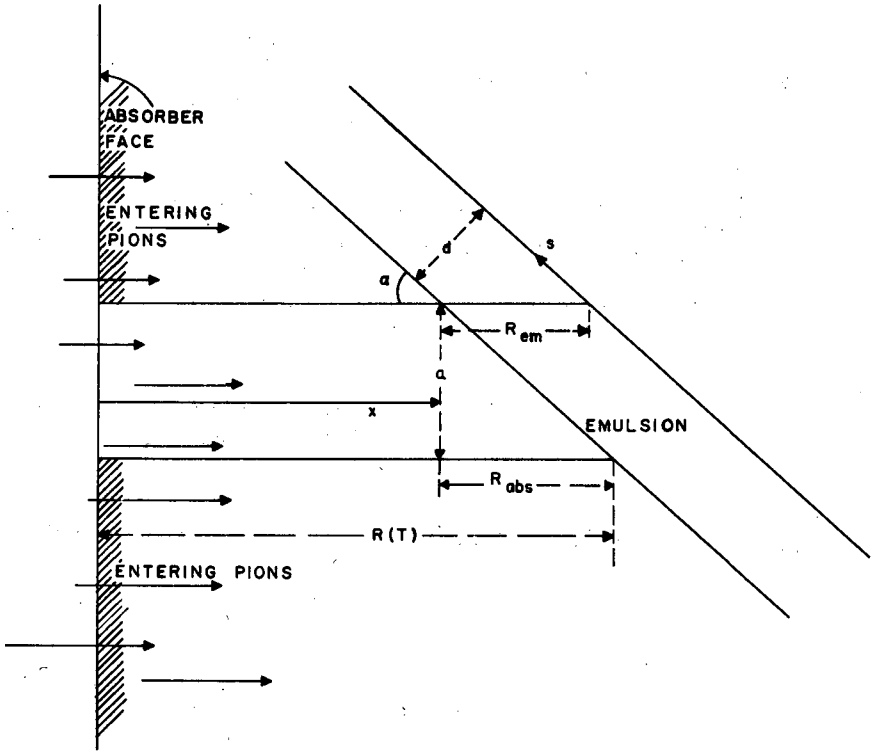

Fig. 9 Pion trajectories in the absorber block.

$$n = N_\pi (T)\, \Delta T\, a \times \ell \qquad (30)$$

since $N_\pi (T)\, \Delta T$ = Number of pions/cm^2 in ΔT and $a \times \ell$ is the cross-sectional area of the beam which comes to rest in the emulsion. We now want to find out over how large a distance along the plate a beam of pions with an energy spread ΔT is distributed. Let s denote the coordinate along the emulsion as shown in Fig. 9. By the use of the well-known relation

$$\Delta T = \left[\frac{dT}{dx}\right]_{abs} \Delta x$$

we immediately obtain that $\Delta T = \left[\frac{dT}{dx}\right]_{abs} \cos \alpha\, \Delta S$

where $\left[\frac{dT}{dx}\right]_{abs}$ is the rate of energy loss of the pion when it enters the absorber face. Substitution of this expression and of Eq. (29) into Eq. (30) above yields

$$n = N_\pi (T) \left[\frac{dT}{dx}\right]_{abs} \left(\frac{R_{abs}}{R_{em}}\right) \ell \times \Delta S \times d$$

where $\ell \times \Delta S$ is the scanned area on the emulsion, and hence we may call the quantity

$$\frac{n}{\ell \times \Delta S \times d} = \rho_\pi = \text{density of pion-track endings in the emulsion.}$$

Finally we thus obtain

$$N_\pi (T) = \frac{\rho_\pi}{\left[\frac{dT}{dx}\right]_{abs} \left(\frac{R_{abs}}{R_{em}}\right)}$$

which is the formula used on page 14.

One additional effect must be considered in connection with the above derivation. This is the possibility of range shortening due to the fact that a thin parallel beam of pions will have experienced a certain lateral spread due to multiple Coulomb scattering by the time it reaches the end of its range. The magnitude of this effect can be calculated from the theory,[12] and one finds that the mean lateral displacement for a 21.6-Mev pion is about 0.085 cm. From this we calculate the mean range shortening and then convert to an energy difference between the real and apparent pion energy. Doing this, one finds this effect to be of the order of 0.05 Mev and hence negligible for our purposes.

2. Derivation of Correction Factors for Cross Section

We shall first calculate the correction which must be applied to allow for the number of pions that decay while in transit from the target to the photographic emulsion:

If dt is a certain time interval in the Lab. then $d\tau = dt\sqrt{1 - v^2/c^2}$ is the time elapsed in the reference system of the pion, where v = the velocity of the pion in the Lab. and c = velocity of light. The time to travel a distance ds is given by

$$d\tau = dt\sqrt{1 - v^2/c^2} = \frac{M}{P}\,ds$$

where ds = distance as measured in Lab.

M = rest mass of pion

P = pion momentum measured in the Lab.

Hence the total time elapsed in traveling from the target to the emulsion is

$$\tau = \left[\int \frac{M}{P}\,ds\right]_{air} + \left[\int \frac{M}{P}\,ds\right]_{abs} \qquad (31)$$

Before the pion reaches the absorber face its momentum is essentially constant and hence the first integral becomes

$$\tau_{air} = \frac{M}{P}\int \rho \, d\phi = \frac{M}{\sqrt{T^2 + 2(Mc^2)\,T}}\,\rho\,\phi$$

where ρ = constant radius of curvature of pion in the magnetic field and

ϕ = angle through which the trajectory turns from the target to the absorber. This time can now be rewritten in the form

$$\tau_{air} = \left(\frac{\rho\phi}{c}\right)\left(\sqrt{\frac{Mc^2}{2T}}\right)\left(\frac{1}{\sqrt{1 + T/2Mc^2}}\right) \text{ (sec)}$$

where T = Kinetic energy of the pion in the laboratory and Mc^2 = its rest mass.

To calculate the time spent by the pion slowing down in the absorber we make the nonrelativistic approximation that $p = \sqrt{2TM}$ and substitute the empirical range-energy relation[13]

$$T = kR^{0.58}$$

We then obtain for the second integral in Eq. (31) the following

$$\tau_{abs} = \int \frac{M}{P}\,ds = \int_0^R \frac{\sqrt{M}\,dR}{\sqrt{2\,k}\,R^{0.29}} = \sqrt{\frac{Mc^2}{2}}\;\frac{R}{R^{0.29}\sqrt{k}}\;\frac{1}{0.71\,C}$$

or $$\tau_{abs} = 4.70 \times 10^{-11}\sqrt{\frac{Mc^2}{2T}}\;R \text{ (sec)}$$

This represents the time for the pion to come to rest after it entered the absorber where R is the range of the pion in question measured in cm.

As a final answer we thus find that the time elapsed in the pion's frame of reference, from its departure from the target until it comes to rest in the emulsion, is given by

$$\tau = \tau_{air} + \tau_{abs} = \left(\frac{\rho\phi}{c}\right)\left(\sqrt{\frac{Mc^2}{2T}}\right)\left(\frac{1}{\sqrt{1+T/2Mc^2}}\right) + 4.70 \times 10^{-11}\sqrt{\frac{Mc^2}{2T}}\ R \text{ (in sec.)}$$

We next want to derive the expression

$$\Delta T = \left[\left(\frac{dT}{dx}\right)_T \Big/ \left(\frac{dT}{dx}\right)_{T'}\right] \Delta T'$$

which appears in the thick-target correction. Consider a pion of energy T' produced at a distance t from the exit surface of the target. We may write this energy as a function of its range R in the target material. The range, in turn, is seen to be equal to $t + R_E(T)$ where $R_E(T)$ is the range of the pion with exit energy T. We may thus write

$$T' = T'(R) = T'\left[t + R_E(T)\right]$$

If we now consider a fixed position t inside the target we can differentiate the above expression for T' considering it to be a function of T only.

$$\frac{dT'}{dT} = \frac{dT'}{dR}\left[\frac{dt}{dT} + \frac{dR_E}{dT}\right] = \frac{dT'}{dR}\frac{dt}{dT} + \frac{dT'}{dR}\frac{dR_E}{dT}$$

But since $\frac{dt}{dT} = 0$ we obtain immediately

$$\Delta T = \left[\left(\frac{dT}{dx}\right)_T \Big/ \left(\frac{dT}{dx}\right)_{T'}\right] \Delta T'$$

This is for a fixed position t inside the target and hence, in order to include all pions produced, we average the quantity $\left(\frac{dT}{dx}\right)_{T'}$ over the thickness of the target. This gives the desired formula

$$\Delta T = \frac{\left(\frac{dT}{dx}\right)_T}{\left(\frac{dT}{dx}\right)_T} \Delta T'$$

VIII REFERENCES

1. K. M. Watson and K. A. Brueckner, Phys. Rev. 83, 1 (1951).

2. K. M. Watson, private communication.

3. W. F. Cartwright, C. Richman, M. N. Whitehead and H. A. Wilcox, Phys. Rev. 91, 677 (1953).

4. R. Mather and E. Segrè, Phys. Rev. 84, 191 (1951).

5. W. H. Barkas, W. Birnbaum and F. M. Smith, Phys. Rev. 91, 765 (1953).

6. W. F. Cartwright, Production of π^+ Mesons by 340-Mev Protons on Protons at 0° to the Beam, Thesis, University of California Radiation Laboratory, Report No. UCRL-1278, April, 1951.

7. C. J. Bakker and E. Segrè, Phys. Rev. 81, 489 (1951).

8. M. Jakobson, A. Schulz and J. Steinberger, Phys. Rev. 81, 894 (1951).

9. D. H. Stork, Total Positive Pion Cross Sections in Complex Nuclei, Thesis, University of California Radiation Laboratory, Report No. UCRL-2288, July, 1953.

10. W. F. Dudziak, private communication.

11. W. A. Aron, The Passage of Charged Particles Through Matter, Thesis, University of California Radiation Laboratory, Report No. UCRL-1325, May, 1951.

12. L. L. Eyges, Phys. Rev. 74, 1534L (1948).

13. H. Bradner, F. M. Smith, W. H. Barkas and A. S. Bishop, Phys. Rev. 77, 462 (1950).